Alexandria Engineering Journal (2021) 60, 4787–4796

HOSTED BY

ELSEVIER

Alexandria University

Alexandria Engineering Journal

www.elsevier.com/locate/aej
www.sciencedirect.com

# Fractional simulation for Darcy-Forchheimer hybrid nanoliquid flow with partial slip over a spinning disk

**Yi-Xia Li** [a], **Taseer Muhammad** [c,d], **Muhammad Bilal** [b], **Muhammad Altaf Khan** [e,f,*], **Ali Ahmadian** [g,h], **Bruno A. Pansera** [h]

[a] *College of Mathematics and Finance, Xiangnan University, Chenzhou 423000, PR China*
[b] *Mathematics Department, City University of Science and Information Technology, Peshawar 25000, Pakistan*
[c] *Department of Mathematics, College of Sciences, King Khalid University, Abha 61413, Saudi Arabia*
[d] *Mathematical Modelling and Applied Computation Research Group (MMAC), Department of Mathematics, King Abdulaziz University, P. O. Box 80203, Jeddah 21589, Saudi Arabia*
[e] *Innstitute for Ground Water Studies, Faculty of Natural and Agricultural Sciences, University of the Free State South Africa, South Africa*
[f] *Department of Mathematics, Faculty of Science and Technology, Universitas Airlangga, Surabaya 60115, Indonesia*
[g] *Institute of IR 4.0, The National University of Malaysia, 43600 Bangi, Selangor, Malaysia*
[h] *Department of Law, Economics and Human Sciences & Decisions Lab, University Mediterranea of Reggio Calabria, Reggio Calabria, Italy*

Received 7 October 2020; revised 21 March 2021; accepted 23 March 2021
Available online 7 April 2021

**KEYWORDS**

FDE12;
Bvp4c;
Caputo derivative;
Hybrid approach;
Slip conditions;
Spinning disk

**Abstract** The present effort elaborates the fractional analyses for Darcy-Forchheimer hybrid nanoliquid flow over a porous spinning disk. Temperature and concentration slip conditions are utilized at the surface of the spinning disk. A specific type of nanoparticles known as Silver-*Ag* and Magnesium-oxide *MgO* is added to the base fluid, to synthesis the hybrid nanoliquid. By using Karman's approach, the system of partial differential equations is depleted into a dimensionless system of differential equations. The obtained equations are further diminished to the first-order differential equation via selecting variables. To develop the fractional solution, the proposed model has been set up by Matlab fractional code Fde12. For accuracy and validity of the resulting framework, the outputs are compared with the fast-approaching numerical Matlab scheme boundary value solver (bvp4c). The impact of several flow constraints versus velocity, mass and thermal energy profiles have been portrayed and discussed. Magnesium oxide *MgO* compound is consists of $Mg^{2+}$ and $O^{2-}$ ions, together bonded by a strong ionic bond, which can be synthesized by pyrolysis of magnesium hydroxide $Mg(OH)_2$ and $MgCO^3$ (magnesium carbonate) at a very high temperature (700–1500 °C). It is more convenient for refractory and electrical applications. Similarly, the antibacterial upshots of silver *Ag* nano-size particles could be used to manage bacterial growth

* Corresponding author.
E-mail address: altafdir@gmail.com (M.A. Khan).

Peer review under responsibility of Faculty of Engineering, Alexandria University.

https://doi.org/10.1016/j.aej.2021.03.062

in several applications, such as dental work, burns and wound treatment, surgery applications and biomedical apparatus.



## 1. Introduction

Hybrid nanoliquid flow over a spinning disk plays an indispensable job in several modern parts encompassing rotors, apparatuses, Psychologist fits, and flywheels. Working as a late revolving disk has a significant piece of businesses, for example, rotor–stator turning circle reactor, warm power creating frameworks, electric-control age, pivoting sawing machines, stopping mechanisms and rotational air cleaner. Shuaib et al. [1] explore the three-dimensional behavior of viscous fluid flow with the heat transmission over the surface of the stretchable non-plate rotating disk. They coupled the Navier Stokes equation along with Maxwell to better illustrate the hydrothermal properties of the fluid, using a numerical parametric continuation approach. The hybrid nanofluid flow consists of magnetic ferrite and carbon nanotubes under the effects of the magnetic field over impermeable an infinite spinning disk is scrutinized by Asifa et al. [2]. It is perceived that the heat transmission rate is significantly improved by the use of nanoparticles in the base fluid. Also, the rising trend in disk rotation positively affects the velocity and temperature of the fluid. Zemedu and Ibrahim [3] studied the two-dimensional, laminar and steady boundary layer flow of micropolar nanoliquid of nonlinear convection due to a spinning disk. They used Matlab numerical package bvp4c for finding results and concluded that the variation in convection parameter raises the fluid velocity, while away from the disk surface opposite scene has been observed. Wakeel et al. [4] has studied the second-grade nanoliquid flow past an expanding disk with thermophoresis, Hall current and Brownian motion influences. The stagnation point flow of Oldroyd-B fluid with mass and heat transport by adopting classical Fourier's law over a porous spinning disk is presented by Hafeez et al. [5]. The nanoliquid flow with the effect of heat dissipation, thermal radiation and Hall current over radially stretching an unsteady spinning disk is considered by Hafeez et al. [6]. They also discussed the numerous features of Lorentz force with the interaction of hybrid nanoliquid motion.

Many scientists have investigated the problems related to nanoliquid from both experimentally and theoretically points of view. However, forming distinct nanoparticles, investigators yield various ingredients to make them. Such nanoparticles contain ceramic oxide, metals, Ferro particles and carbon in various forms (diamonds, graphite, and carbon nanotubes). While some sort of nanoliquid named hybrid nanoliquids is presented which is supposed to propose superior thermos-physical characteristics and excellent rheological behavior with enriched heat transport features. Hybrid nanofluid has been widely used in various sectors of heat transport like micro-electric and generator cooling, cooling of the atomic system, reduction of drugs, refrigeration, cooling of the transformer, and many more. The concept of hybrid nanofluid to more improve the progressive features of ordinary nanofluid was introduced by Suresh [7]. Khan et al. [8] has conducted a theoretical study on MHD rotating flow consist of hybrid nanoparticles with thermal and velocity slips conditions between two parallel plates. The stability analysis by using bvp4c of copper aluminum oxides $Cu$-$Al_2O_3$/Water nanoliquid having suction and radiation effects over a shrinking rotating disk is calculated by Anuar et al. [9]. Zhang et al. [10] prepared poly magnesium oxide PBAT/($MgO$-$Ag$) or (butylene adipate-co-terephthalate) via a casting procedure for food packing and preservation. The impact of ($MgO$-$Ag$) nanoparticles on the antibacterial and physical characteristics of composite biofilms are also investigated. Gulati et al. [11] presented a porous 3D model for magnesium-oxide $MgO$ and $Ag$(noble metal) nanoparticles used for the insertion of $CO_2$ alkyne components. Their outputs revealed that a $CO_2$ substrate and captures the main role for 3D porous $MgO$, while $Ag$ plays the key activation of $CO_2$ and alkyne insertion steps. Saravanakumar Cytotoxicity illustrated that the $Ag$-$MgO$ is stronger in inducing prostate cancer (PC-3) cell death as compared to the $MgO$. Therefore, it can be concluded that the $Ag$-$MgO$ would be potential therapeutics for cancer treatment [12]. Goyal *et al.* [13] simulated the numerical solution for AIDS/HIV transfer model. Gao et al. [14] constructed an approximate out-comes for AIDS/HIV transfer model, while considering fractional transform method.

The signal processing, anomalous diffusion transport, in porous material the fluid flow, in viscoelastic materials the wave propagation, biological system's electric conductance and financial theory, the fractional calculus describe almost all phenomena in applied sciences. Salem et al. [15] monitored the uniqueness and existence of the system of fractional Langevin nonlinear equations with the nonlocal and multipoint integral condition, by manipulating Caputo's non-integer order derivative. While using Banach's fixed-point theorem, they find out the uniqueness of the concerned problem. Baleanu et al. [16] presented a new non-integer order model based on Caputo-Fabrizio derivative for the human liver with the exponential kernel. The unique solution existence is investigated by

**Table 1** The numerical properties of water and hybrid nanofluid [30,31].

| | $\rho(kg/m^3)$ | $C_p(j/kgK)$ | $k(W/mK)$ | $\beta \times 10^5(K^{-1})$ | $Pr$ |
|---|---|---|---|---|---|
| Pure water | 997.1 | 4179 | 0.613 | 21 | 6.2 |
| Magnesium oxide | 3560 | 955 | 45 | 1.80 | |
| Silver | 10,500 | 235 | 429 | 1.89 | |

making use of the fixed-point theory and Picard–Lindelöf concept. The time-dependent viscous fluid flow with thermo-diffusive effects and heat and mass transmission characteristics over a flexible spinning disk, by using the Caputo approach is scrutinized by Shuaib et al. [17]. Tuan et al. [18] presented the COVID-19 transmission model by Caputo non-integer order derivative. They employed the Adams-Bashforth-Moulton technique for the approximate solution of the problem and calculated the reproduction number and equilibrium point. Akram et al. [19] calculated the numerical results for time-fractional second-order equations. A collocation concept based on cubic B-spline function, to investigate the approximate solution of the problem using time fractional derivative is examined by Khalid et al. [20]. Jena et al. [21] studied a semi-analytical technique known as fractional reduced transform method for the solution of Schrodinger type principal model. Khalid et al. [22] and Akram et al. [23] scrutinized a redefined B-spline function based on finite difference scheme. They considered redefined B-spline function and Caputo fractional derivative for spatial discretization. Ameen et al. [24] formulated the SIRV model as a system of non-integer order differential equations using Caputo derivative. Gao et al. [25] investigated a numerical solution for disease in pregnant women using fractional definition. Using the reliable space, Al-Refai [26] considered the results for nonlinear fractional differential equations.

The intention behind the present work is to elaborate the fractional analyses for Darcy-Forchheimer hybrid nanoliquid flow with a porous medium and extend the idea of Ref. [27]. The hybrid nanoliquid is synthesis in the presence of special type nanomaterial's known as Silver and magnesium oxide nanoparticles. By using an appropriate transformation, the system of partial differential equations is depleted into a dimensionless system of ordinary differential equations. To develop the fractional solution, the proposed model has been set up by Matlab fractional code FDE12. For accuracy and validity of the resulting framework, the outputs are compared with fast approaching numerical Matlab scheme bvp4c. The impact of several flow constraints versus velocity, mass and thermal energy profiles have been drawn and discussed.

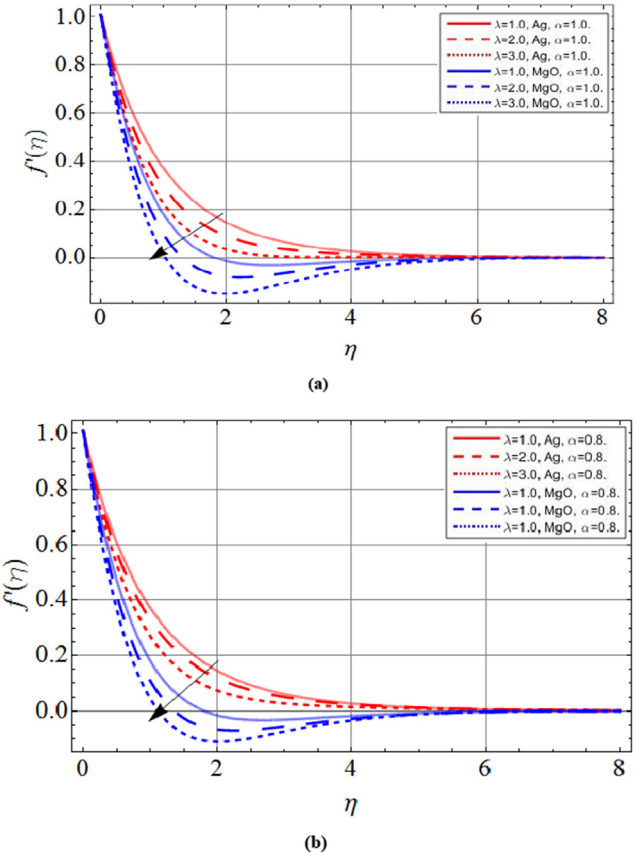


**Fig. 2** Axial velocity profile $f'(\eta)$ versus a parameter $\lambda$. When $\alpha = 1.0$, $\mathrm{Pr} = 6.2$, $\beta = 0.5$, $Fr = 1.0$, $Ec = 2.0$, $Sc = 0.3$, $\phi_1 = \phi_2 = 0.01$.

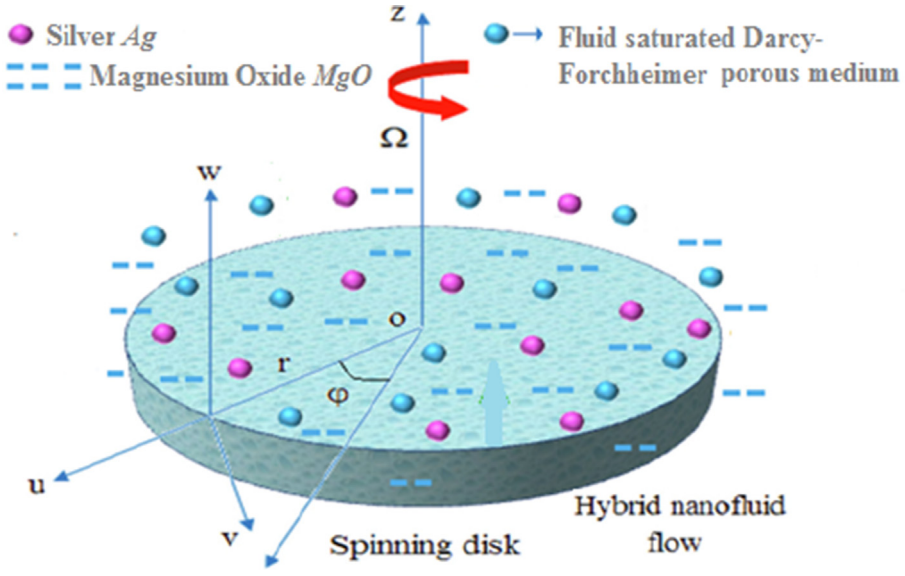


**Fig.1** Physical sketch of the spinning cone.

## 2. Mathematical formulation

We illustrate three-dimensional steady Darcy-Forchheimer hybrid nanoliquid flow with thermal and concentration slips conditions at the surface of the spinning disk. The disk revolves with the angular velocity $\Omega$ at the $z$-axis. The velocity component $u$, $v$ and $w$ have been assumed along $r$, $\varphi$, $z$ the direction. The boundary layer equations are [2,27]:

$$\frac{\partial u}{\partial x}+\frac{\partial w}{\partial z}+\frac{u}{r}=0, \tag{1}$$

$$u\frac{\partial u}{\partial r}+w\frac{\partial u}{\partial z}-\frac{v^2}{r}=\nu_{hnf}\left(\frac{\partial^2 u}{\partial z^2}+\frac{\partial^2 u}{\partial r^2}+\frac{1}{r}\frac{\partial u}{\partial r}-\frac{u}{r^2}\right)-\nu_{hnf}\frac{u}{k^*}-Fu^2, \tag{2}$$

$$u\frac{\partial v}{\partial r}+w\frac{\partial v}{\partial z}+\frac{vu}{r}=\nu_{hnf}\left(\frac{\partial^2 v}{\partial z^2}+\frac{\partial^2 v}{\partial r^2}+\frac{1}{r}\frac{\partial v}{\partial r}-\frac{v}{r^2}\right)-\nu_{hnf}\frac{v}{k^*}-Fv^2, \tag{3}$$

$$u\frac{\partial w}{\partial r}+w\frac{\partial w}{\partial z}=\nu_{hnf}\left(\frac{\partial^2 w}{\partial z^2}+\frac{\partial^2 w}{\partial r^2}+\frac{1}{r}\frac{\partial w}{\partial r}\right)-\nu_{hnf}\frac{w}{k^*}-Fw^2, \tag{4}$$

$$(\rho C_p)_{hnf}u\frac{\partial T}{\partial r}+w\frac{\partial T}{\partial z}=k_{hnf}\frac{\partial^2 T}{\partial z^2}+\mu_{hnf}\left[\left(\frac{\partial u}{\partial z}\right)^2+\left(\frac{\partial v}{\partial z}\right)^2\right], \tag{5}$$

$$u\frac{\partial C}{\partial r}+w\frac{\partial C}{\partial z}=D_{hnf}\frac{\partial^2 C}{\partial z^2}. \tag{6}$$

The boundary condition for the above flow problem is defined as:

$$\left.\begin{aligned} u=r\Omega,\ v=r\Omega,\ w=0,\ T=T_w+L_1\tfrac{\partial T}{\partial z},\ C=C_w+L_2\tfrac{\partial C}{\partial z}\ \text{ at } z=0,\\ u\to 0,\ v\to 0,\ w\to 0,\ T\to T_\infty,\ C\to C_\infty\ \text{ as } z\to\infty. \end{aligned}\right\} \tag{7}$$

where $\rho_{hnf}$, $\mu_{hnf}$ and $\nu_{hnf}$ show density, dynamic viscosity and kinematic viscosity of hybrid nanoliquid respectively. $L_1$ Thermal slip factor, $L_2$ concentration slip factor, $\alpha^*=(\rho c)_{hnf}$ the thermal diffusivity, $k$ the thermal conductivity, $C$ is concentration, $C_\infty$ ambient concentration, $T$ is temperature, $T_\infty$ ambient temperature and $D_{hnf}$ is the hybrid nanofluid mass diffusivity.

In order to transform the above system of modeled equations (1–7) we introduce the following similarity approach [28]:

$$\left.\begin{aligned} u=r\Omega f'(\eta),\ v=r\Omega g(\eta),\ w=-(2\Omega\nu)^{1/2}f(\eta),\ \eta=\left(\frac{2\Omega}{\nu}\right)^{1/2}z,\ \Phi=\frac{C-C_\infty}{C_w-C_\infty},\ \Theta=\frac{T-T_\infty}{T_w-T_\infty}. \end{aligned}\right\} \tag{8}$$

By making use of Eq. (8) in Eqs. (1)–(7), we get the following system of ordinary differential equations:

$$2f'''+\frac{\mu_{hnf}}{\mu_f}\left[2ff''-f'^2-\lambda f'+g^2-Frf'^2\right]=0, \tag{9}$$

$$2g''+\frac{\mu_{hnf}}{\mu_f}\frac{\rho_{hnf}}{\rho_f}\left[2fg'-2f'g-\lambda g-Frg^2\right]=0, \tag{10}$$

$$\frac{k_{hnf}}{k_f}\Theta''-\Pr\frac{(\rho Cp)_{hnf}}{(\rho Cp)_f}[f\Theta']+Ec\left((f'')^2+(g')^2\right)=0, \tag{11}$$

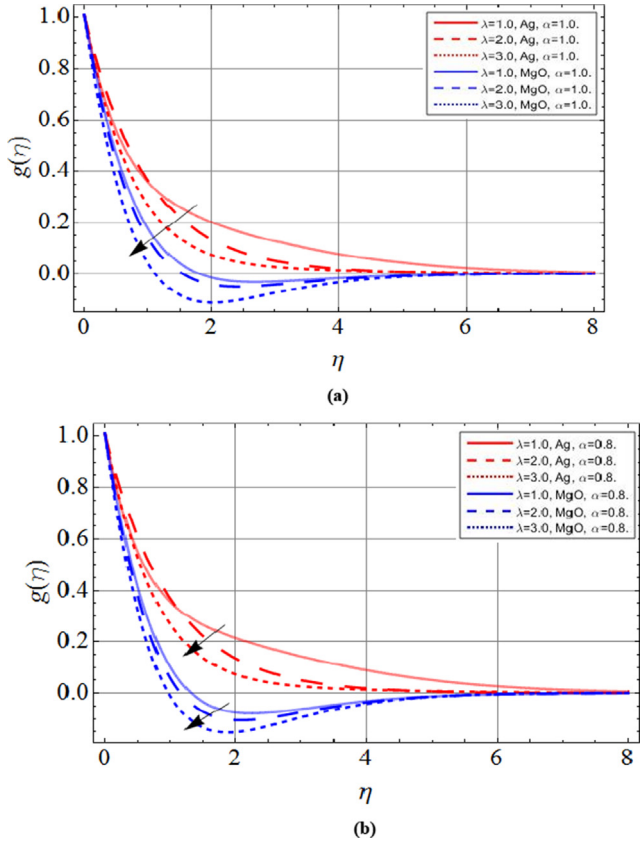


**Fig. 3** Radial velocity profile $g'(\eta)$ versus a parameter $\lambda$. When $\alpha=1.0$, $\Pr=6.2$, $\beta=0.5$, $Fr=1.0$, $Ec=2.0$, $Sc=0.3$, $\phi_1=\phi_2=0.01$.

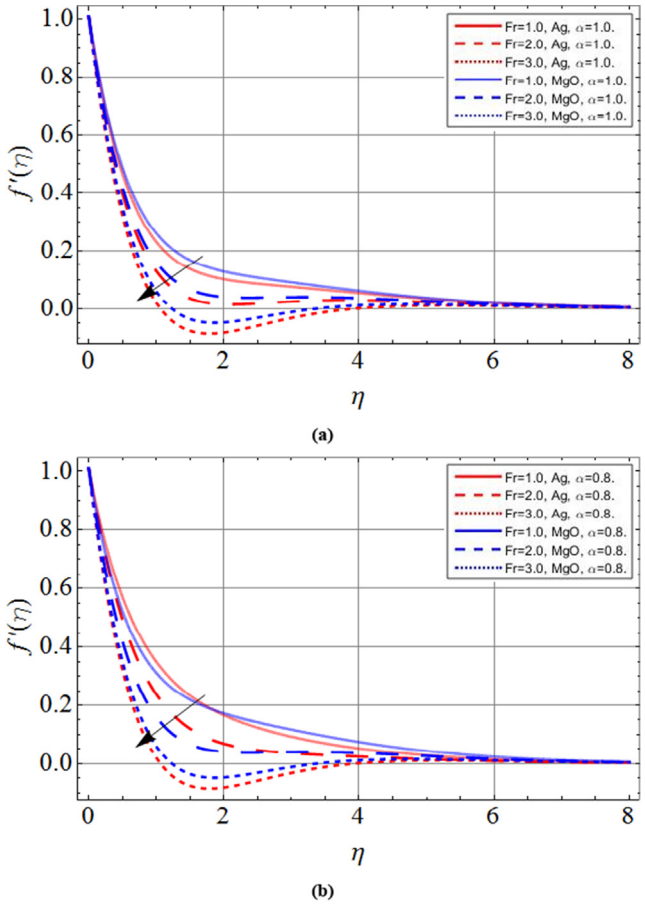


**Fig. 4** Axial velocity profile $f'(\eta)$ versus parameter $Fr$. When $\alpha=1.0$, $\Pr=6.2$, $\beta=0.5$, $\lambda=2.0$, $Ec=2.0$, $Sc=0.3$, $\phi_1=\phi_2=0.01$.

$$\Phi'' - Sc[f\Phi'] = 0. \tag{12}$$

$$\left.\begin{array}{c} f(0)=0, f'(0)=1, g(0)=1, \Theta(0)=1+\beta\Theta'(0), \Phi(0)=1+\gamma\Phi'(0), \\ f'(\infty)\to 0, g(\infty)\to 0, \Theta(\infty)\to 0, \Phi(\infty)\to 0 \end{array}\right\} \tag{13}$$

The dimensionless numbers that appear in the above equations are expressed as:

$$\left.\begin{array}{c} \mathrm{Pr}_{hnf}=\frac{(\mu C_p)_{hnf}}{k_{hnf}}, \lambda=\frac{\nu}{k^*\Omega}, Ec=\frac{\Omega^2 r^2}{c_p\Delta T}, Sc=\frac{\nu_f}{D_f}, \\ Fr=\frac{C_b}{k^{*1/2}}, \beta=L_1\sqrt{\frac{2\Omega}{\nu}}, \gamma=L_2\sqrt{\frac{2\Omega}{\nu}}. \end{array}\right\} \tag{14}$$

where $Pr$ is the Prandtl number, $\lambda$ the porosity parameter, $Ec$ the Eckert number, $Sc$ the Schmidt number and $Fr$ is the Forchheimer term. While $\beta$ and $\gamma$ is the thermal slip and concentration slip parameters respectively.

### 2.1. Thermophysical properties of nanoliquid

The specific heat capacity and the density of the hybrid nanoliquid can be expressed as [29]:

$$(\rho C_p)_{hnf} = \left\{(1-\phi_2)\left[(1-\phi_1)(\rho C_p)_f + \phi_1(\rho C_p)_{s1}\right]\right\} + \phi_2(\rho C_p)_{s2} \tag{15}$$

$$\rho_{hnf} = \left\{(1-\phi_2)\left[(1-\phi_1)_{\rho_f} + \phi_1\rho_{s1}\right]\right\} + \phi_2\rho_{s2}, \tag{16}$$

where $\rho_{s1}, \rho_{s2}$ are the density, $(C_p)_{s1}, (C_p)_{s2}$ are specific heat capacity and $\phi_1$, $\phi_2$ are the volume fraction of the silver and magnesium oxide nanoliquid respectively, which are mentioned in Table 1. While the thermal diffusivity, thermal conductivity, effective viscosity $\mu_{hnf}$ and effective thermal conductivity of hybrid nanofluid is calculated by curve fitting on real experimental data [28,29].

$$\left.\begin{array}{c} \alpha_{hnf}=\frac{k_{hnf}}{(\rho C_p)_{hnf}}, \\ k_{hnf}=-\frac{q_w}{\partial\theta/\partial y}, \\ k_{hnf}=\left(\frac{0.1747\times10^5+\phi}{0.1747\times10^5-0.1498\times10^6\phi+0.1117\times10^7\phi^2+0.1997\times10^8\times\phi^3}\right)k_f, \\ \mu_{hnf}=\left(1+2.5\varphi_1+6.2\varphi_2^2\right)\mu_f. \end{array}\right\} \tag{17}$$

The drag force, Nusselt numbers and Sherwood numbers are defined as [27]:

$$Re_r^{1/2}C_f = f''(0),\ Re_r^{1/2}C_g = g'(0),\ Re_r^{-1/2}Nu = -\Theta'(0),\ Re_r^{-1/2}Sh = -\Phi'(0). \tag{18}$$

where, $Re_r = \Omega r^2/\nu_f$, is the local rotational Reynolds number.

## 3. Preliminaries

**Definition 1..** The fractional integral of order $\alpha \succ 0$ for a function $h : R^+ \to R$ is defined as:

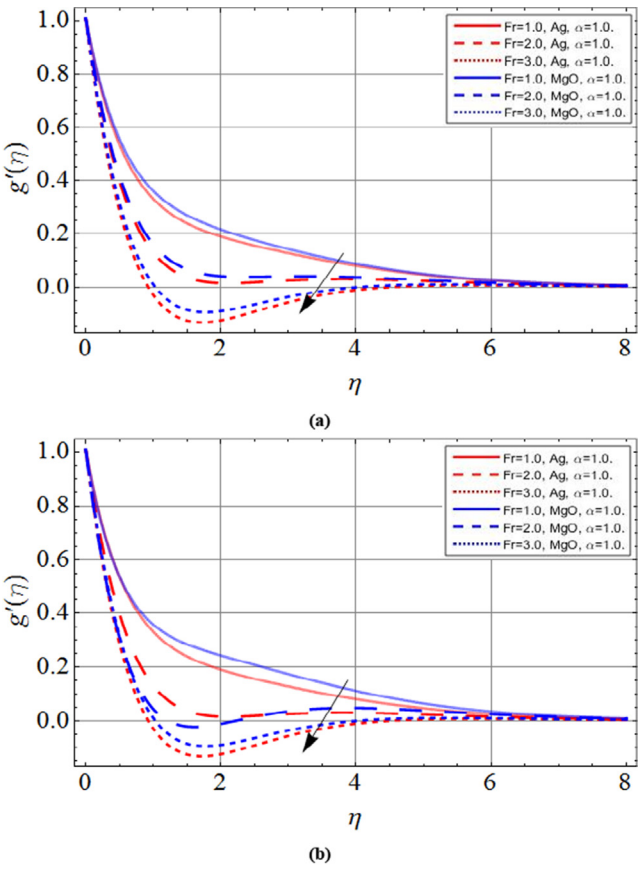


**Fig. 5** Radial velocity profile $g'(\eta)$ versus parameter $Fr$. When $\alpha = 1.0$, Pr = 6.2, $\beta = 0.5$, $\lambda = 2.0, Ec = 2.0$, $Sc = 0.3$, $\phi_1 = \phi_2 = 0.01$.

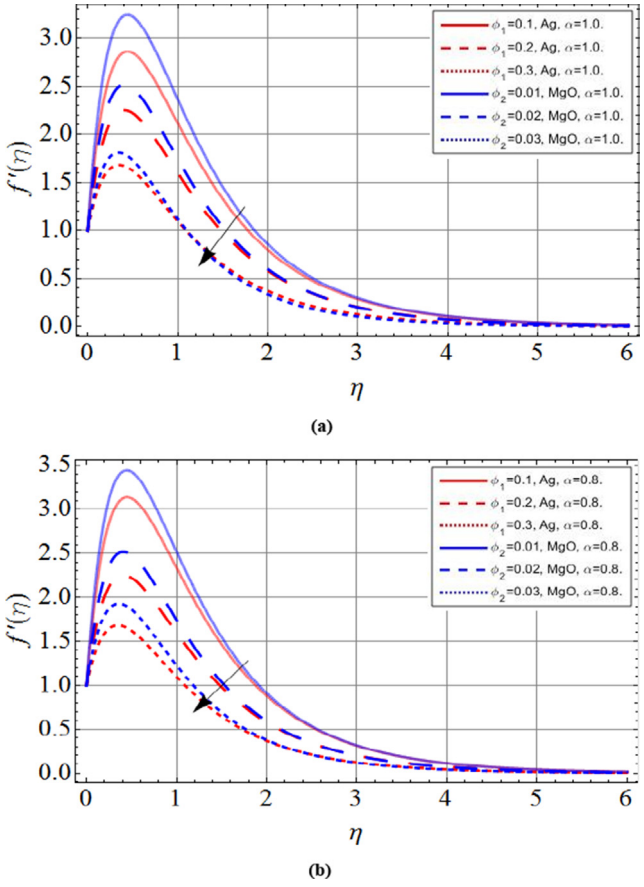


**Fig. 6** Axial velocity profile $f'(\eta)$ versus a parameter $(\phi_1, \phi_2)$. When $\alpha = 1.0$, Pr = 6.2, $\beta = 0.5$, $\lambda = 2.0$, $Fr = 1.0$, $Ec = 2.0$, $Sc = 0.3$.

$$I_{\eta}^{\alpha}(h(\eta)) = \frac{1}{\Gamma(\alpha)} \int (\eta - \chi)^{\alpha-1} h(\chi) d\chi. \tag{19}$$

**Definition 2.** *The Caputo derivative for a function $h \in C^n$ of order $\alpha$ is*:

$$^{c}D_{\eta}^{\alpha}(h(\eta)) = \frac{1}{\Gamma(n-\alpha)} \int_0^t \frac{h^n(\chi)}{(\eta-\chi)^{\alpha-n+1}} d\chi, n-1 \prec \alpha \prec n \in N. \tag{20}$$

Clearly $^{c}D_{\eta}^{\alpha}(h(\eta))$ tends to $h'(\eta)$ as $\alpha \to 1$.

## 4. Problem solution

The following variables are selected, in order to deplete the system of high order differential equations (9)–(12) and (13):

$$\left.\begin{array}{c} \eta = \zeta_1, f = \zeta_2, f' = \zeta_3, f'' = \zeta_4, g = \zeta_5, g' = \zeta_6, \Theta = \zeta_7, \Theta' = \zeta_8, \\ \Phi = \zeta_9, \Phi' = \zeta_{10}. \end{array}\right\} \tag{21}$$

$$\left\{\begin{array}{c} \zeta_1' = 1, \zeta_2' = \zeta_3, \zeta_3'' = \zeta_4 \\ \zeta_4' = \frac{1}{2}\left\{-\zeta_2\zeta_4 + \zeta_3^2 + \lambda\zeta_3 - \zeta_5^2 + Fr\zeta_3^2\right\}, \\ \zeta_5' = \zeta_6, \zeta_6' = \frac{1}{2}\left(\lambda\zeta_5 + Fr\zeta_5^2\right) - \zeta_2\zeta_6 + \zeta_3\zeta_5, \zeta_7' = \zeta_8, \\ \zeta_8' = \Pr(\zeta_2\zeta_8) - Ec\left((\zeta_3)^2 + (\zeta_6)^2\right), \\ \zeta_9' = \zeta_{10}, \zeta_{10}' = Sc(\zeta_2\zeta_{10}). \end{array}\right. \tag{22}$$

Now to generalize the above system of a first-order differential equation, we apply the definition of Caputo fractional derivative; as a result, we get the following noninteger order differential equations:

$$\left\{\begin{array}{c} D_t^{\alpha}\zeta_1 = 1, {}_{t}^{\alpha}\zeta_2 = \zeta_3, \mathrm{D}_{t}^{\alpha}\zeta_3 = \zeta_4 \\ D_t^{\alpha}\zeta_4 = \frac{1}{2}\left\{-\zeta_2\zeta_4 + \zeta_3^2 + \lambda\zeta_3 - \zeta_5^2 + \mathrm{Fr}\zeta_3^2\right\}, \\ D_t^{\alpha}\zeta_5 = \zeta_6, \mathrm{D}_{t}^{\alpha}\zeta_6 = \frac{1}{2}\left(\lambda\zeta_5 + \mathrm{Fr}\zeta_5^2\right) - \zeta_2\zeta_6 + \zeta_3\zeta_5, \\ D_t^{\alpha}\zeta_7 = \zeta_8, \mathrm{D}_{t}^{\alpha}\zeta_8 = \mathrm{Pr}(\zeta_2\zeta_8) - \mathrm{Ec}\left((\zeta_3)^2 + (\zeta_6)^2\right), \\ D_t^{\alpha}\zeta_9 = \zeta_{10}, {}_{t}^{\alpha}\zeta_{10} = \mathrm{Sc}(\zeta_2\zeta_{10}). \end{array}\right. \tag{23}$$

The boundary conditions are:

$$\left.\begin{array}{c} \zeta_2(0) = 0, \zeta_3(0) = \zeta_4, \zeta_5(0) = 1 + \zeta_6, \zeta_7(0) = 1 + \beta, \zeta_9(0) = 1 + \gamma\zeta_{10}, \\ \zeta_3(\infty) \to 0, \zeta_5(\infty) \to 0, \zeta_7(\infty) \to 0, \zeta_9(\infty) \to 0 \end{array}\right\} \tag{24}$$

## 5. Result and discussion

The motivation behind this portion is to determine and disused the performance of the temperature, velocity and mass transfer rate versus different physical parameters. The results are obtained through Matlab fractional package (Fde12) and for the validity and accuracy of the outcomes, a fast-approaching numerical scheme, boundary value solver (bvp4c) has been implemented. Figs. 2–12(a) display the comparison of Silver and Magnesium-oxide nanoliquid behavior at $a$ = 1,

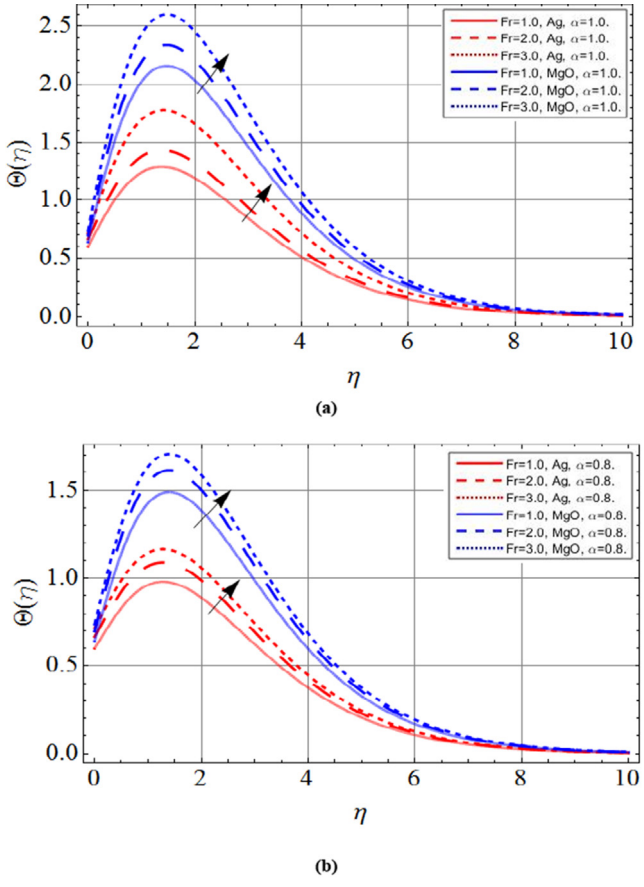


**Fig. 7** Temperature profile $\theta(\eta)$ versus a parameter $Fr$. When $\alpha = 1.0$, $\Pr = 6.2$, $\beta = 0.5$, $\lambda = 2.0$, $Ec = 2.0$, $Sc = 0.3$, $\phi_1 = \phi_2 = 0.01$.

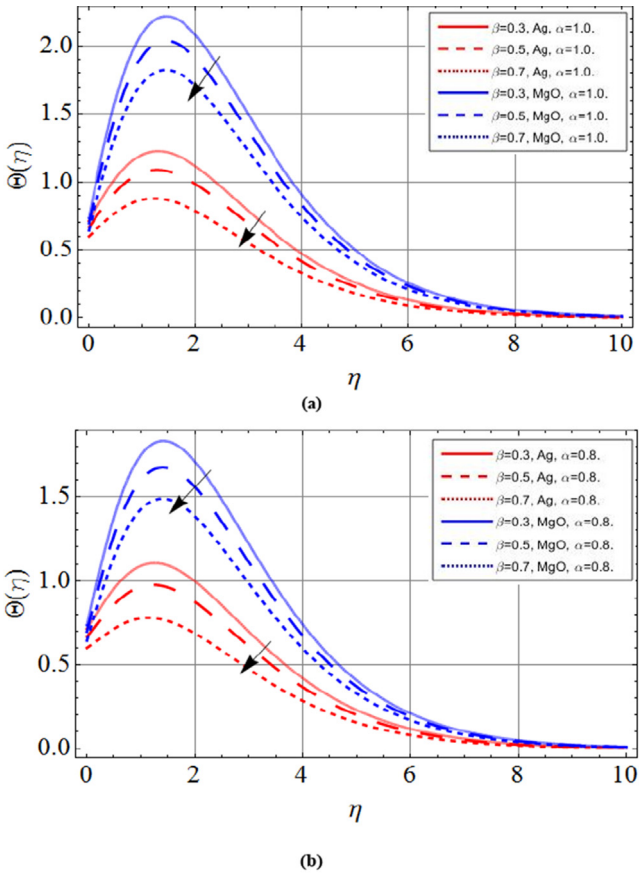


**Fig. 8** Temperature profile $\theta(\eta)$ versus parameter $\beta$. When $\alpha = 1.0$, $\Pr = 6.2$, $\lambda = 2.0$, $Fr = 1.0$, $Ec = 2.0$, $Sc = 0.3$, $\phi_1 = \phi_2 = 0.01$.

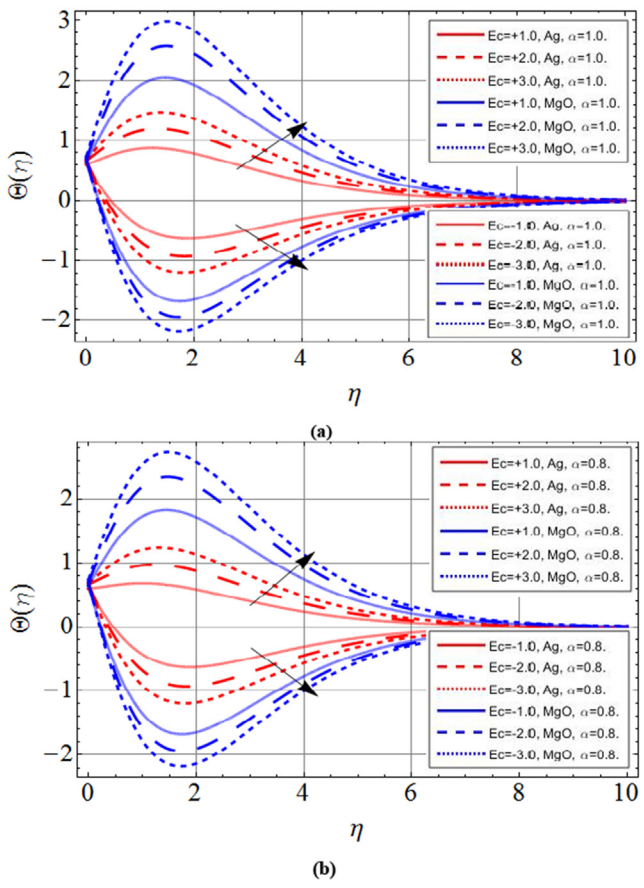


**Fig. 9** Temperature profile $\theta(\eta)$ versus parameter $Ec$. When $\alpha = 1.0$, Pr = 6.2, $\beta = 0.5$, $\lambda = 2.0$, $Fr = 1.0$, $Sc = 0.3$, $\phi_1 = \phi_2 = 0.01$.

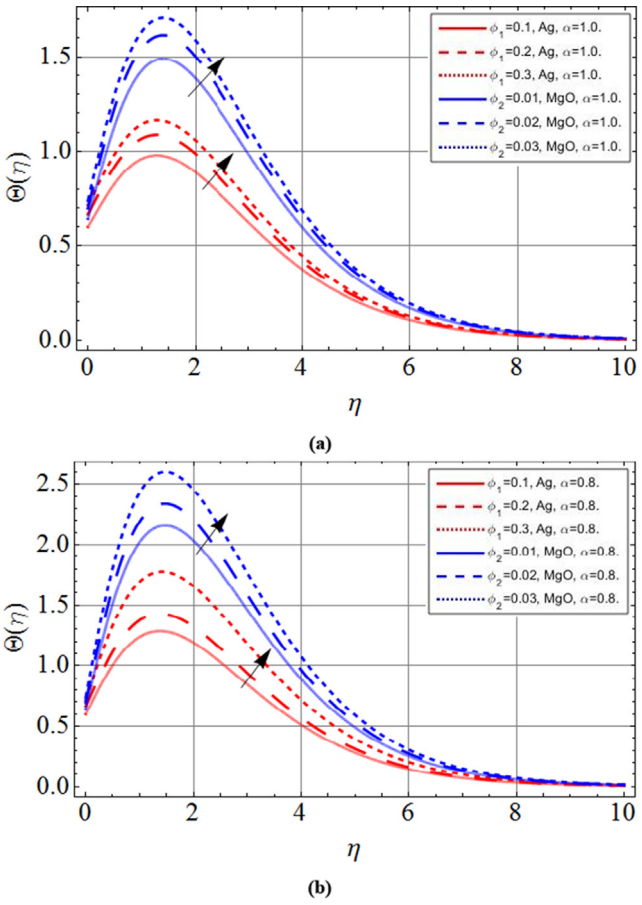


**Fig. 10** Temperature profile $\theta(\eta)$ versus a parameter $(\phi_1, \phi_2)$. When $\alpha = 1.0$, Pr = 6.2, $\beta = 0.5$, $\lambda = 2.0$, $Fr = 1.0$, $Ec = 2.0$, $Sc = 0.3$.

while Figs. 2-12(b) revealed the fractional behavior of nanoliquid at $a = 0.8$. Fig. 1 shows the physical mechanism of hybrid nanoliquid flow over a porous spinning disk.

Figs. 2 and 3 revealed the dominance of porosity parameter $\lambda$ versus axial velocity $f'(\eta)$ and radial velocity $g'(\eta)$ profiles respectively. The rising trend of porosity term $\lambda$ reduces the flow field because the suction/injection takes place with the variation of $\lambda$, which resist to the flow field. Figs. 4 and 5 scrutinized the influence of Forchheimer term $Fr$ on axial velocity $f'(\eta)$ and radial velocity $g'(\eta)$ profiles respectively. The increment in Forchheimer term $Fr$ decreases the fluid velocity. The porous surface permeability declines with a rising trend of Forchheimer term $Fr$. Which minimizes the velocity profiles of both Silver and Magnesium-oxide nanoliquid.

Fig. 6 communicates the volume friction parameters'$(\phi_1, \phi_2)$ effect on the axial velocity profile. The addition of nanoparticles in base fluid significantly enhances the viscosity of the fluid, while reduces the thermal expansion of the fluid, that's why the fluid velocity decreases with the variation of volume friction parameters $(\phi_1, \phi_2)$. The growing values of Forchheimer term $Fr$ enhance the fluid temperature $\theta(\eta)$ shown in Fig. 7. Fig. 8 illustrates the thermal slip parameter $\beta$ influence on the temperature field $\theta(\eta)$. The slip effects reduce the friction force; these forces oppose the flow field and were the main agent for enhancing the temperature rate. That's why the temperature field declines with thermal slip parameter $\beta$ effects.

Fig. 9 displays the temperature field behavior versus Eckert number $Ec$. The Eckert effects embody the internal kinematic energy to heat energy against the viscous stresses. This energy causes the enhancement of fluid temperature. The volume friction parameters $(\phi_1, \phi_2)$ influence on temperature profile is presented via Fig. 10. The increment in the number of nanoparticles increases the viscosity of the base fluid, which opposes the flow field. This resistive force enhances the fluid temperature $\theta(\eta)$. Fig. 11 illustrates the concentration transfer behavior versus Schmidt number $Sc$. The kinematic viscosity of fluid enhances the rising trend of Schmidt number, that's why mass a transfer rate decrease with Schmidt number Sc. Fig. 12 presents the total residual error. While Figs. 13 and 14 are drawn to display the error analysis of Forchheimer term $Fr$ and volume friction parameter $\phi_1$. Table 1 illustrates the physical geometry of the problem. Tables 2, 3 and 5 display the validity of the results with the existing literature. While table 4 shows the comparison of fractional method FDE12 and bvp4c. The

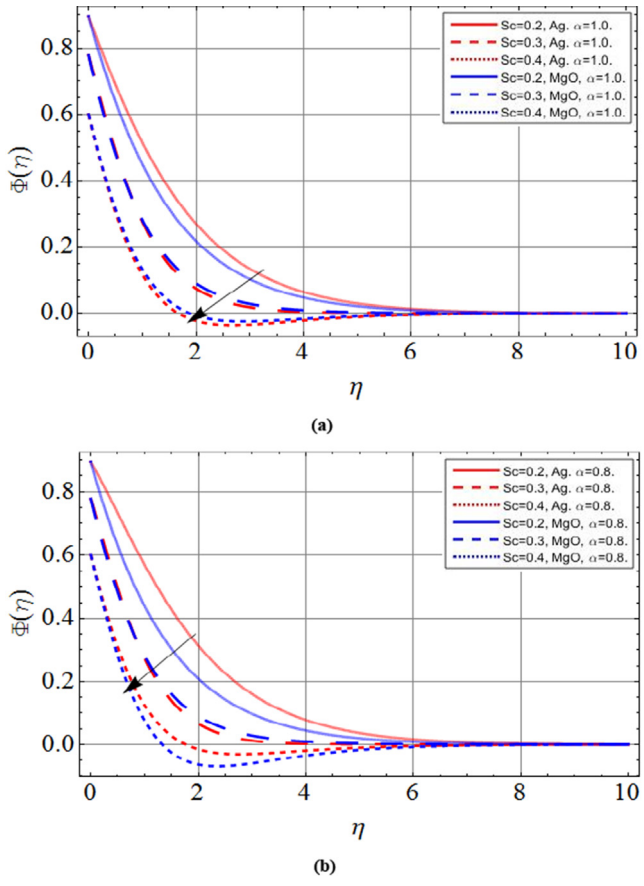


**Fig. 11** Concentration profile $\Phi(\eta)$ versus parameter $Sc$. When $\alpha = 1.0$, Pr = 6.2, $\beta = 0.5$, $\lambda = 2.0$, $Fr = 1.0$, $Ec = 2.0\,\phi_1 = \phi_2 = 0.01$.

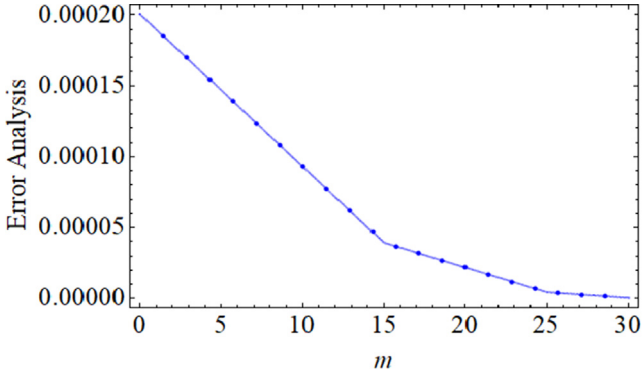


**Fig. 12** Total square residual error $\varepsilon_m^t$ when $\lambda = 2.0$, $\phi_1 = 0.02$, $Fr = 1.0, \phi_2 = 0.2, \beta = 0.5, Ec = 2, Sc = 3$, Pr = 6.2.

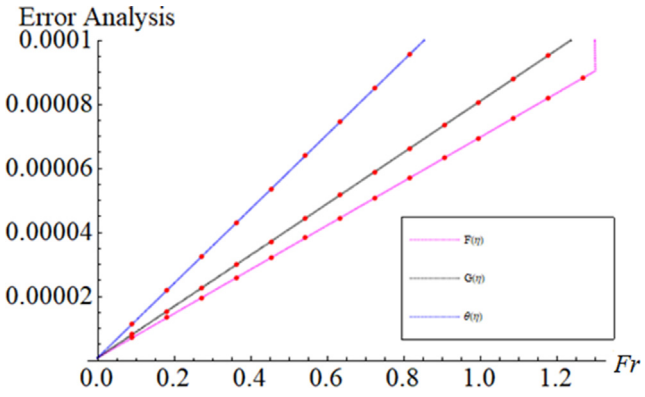


**Fig. 13** Range of the parameter $Fr$ When $\phi_2 = 0.2$, $\lambda = 2.0$, $\phi_1 = 0.02, \beta = 0.5, Ec = 2$, $Pr = 6.2$, $Sc = 2.0$.

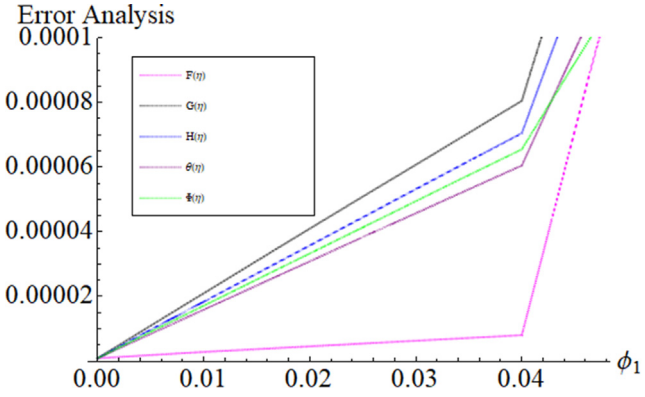


**Fig. 14** Range of the parameter $\phi_1$ When $Fr = 1.0$, $\lambda = 2.0$, $\phi_2 = 0.2$, $Ec = 2$, $\mathrm{P}r = 6.2$, $Sc = 3$.

**Table 2** The numerical comparison for skin friction with the existing literature, while keeping $\alpha = 1.0$, Pr = 6.2, $\beta = 0.5$, $\lambda =$, $Fr = 1.0$, $Ec = 2.0$, $Sc = 0.3$, $\phi_1 = \phi_2 = 0.01$.

| $\beta$ | Hamad et al. [32] | Ramya et al. [33] | Present work |
|---|---|---|---|
| 0.0 | 0.6283 | 0.6283 | 0.6283 |
| 0.2 | 0.7674 | 0.7675 | 0.7677 |
| 0.5 | 0.8901 | 0.8901 | 0.8922 |
| 1.0 | 1.0004 | 1.0005 | 1.0009 |
| 3.0 | 1.1489 | 1.1490 | 1.1493 |
| 10 | 1.2352 | 1.2352 | 1.2361 |
| 20 | 1.2577 | 1.2578 | 1.2582 |

## 6. Conclusion

In this work, the fractional analyses for Darcy-Forchheimer hybrid nanoliquid flow with temperature and concentration slip conditions over a porous spinning surface have been studied. Silver $Ag$ and Magnesium-oxide $MgO$ nanoparticles are used for the synthetization of hybrid nanoliquid. Magnesium oxide $MgO$ compound is consists of $Mg^{2+}$ and $O^{2-}$ ions, together bonded by a strong ionic bond, which can be synthesized by pyrolysis of magnesium hydroxide $Mg\ (OH)^{\ 2}$ and $MgCO^3$ (magnesium carbonate) at a very high temperature (700–1500 °C). It is more convenient for refractory and electrical applications. Similarly, the antibacterial upshots of silver $Ag$ nano-size particles have been used to manage bacterial growth in several applications, such as dental work, burns and wound treatment, surgery applications and biomedical apparatus. Keeping in view the above applications the present problem has modeled. By using the similarity concept, the system of nonlinear partial differential equations is lessened to the dimensionless system of differential equations. The obtained

**Table 3** The numerical comparison for $-\theta'(0)$ and $-\Phi'(0)$ with the existing literature, while keeping $\alpha = 1.0$, Pr = 6.2, $\beta = 0.5$, $\lambda =$, $Fr = 1.0$, $Ec = 2.0$, $Sc = 0.3$, $\phi_1 = \phi_2 = 0.01$.

| | | Ramya et al. [33] | Present work | Ramya et al. [33] | Present work |
|---|---|---|---|---|---|
| *Pr* | *Sc* | $-\theta'(0)$ | $-\theta'(0)$ | $-\Phi'(0)$ | $-\Phi'(0)$ |
| 6.2 | | 3.7715 | 3.7717 | | |
| 6.3 | | 3.2514 | 3.2579 | | |
| 6.4 | | 2.8278 | 2.8280 | | |
| | 0.2 | | | 5.6212 | 5.6215 |
| | 0.3 | | | 0.9977 | 0.9980 |
| | 0.4 | | | 0.4521 | 0.4527 |

**Table 4** The numerical comparison for $f'(0)$, $g(0)$ and $\Theta(0)$ between Fde12 and bvp4c, while keeping $\alpha = 1.0$, Pr = 6.2, $\beta = 0.5$, $\lambda =$, $Fr = 1.0$, $Ec = 2.0$, $Sc = 0.3$, $\phi_1 = 0.01$.

| | Fde12 | bvp4c | Fde12 | bvp4c | Fde12 | bvp4c | Computational cost |
|---|---|---|---|---|---|---|---|
| $\phi_2$ | $f'(0)$ | $f'(0)$ | $g(0)$ | $g(0)$ | $\Theta(0)$ | $\Theta(0)$ | bvp4c |
| 0.00 | 1.0000 | 1.0000 | 1.0000 | 1.0000 | 0.8700 | 0.8730 | |
| 0.02 | 0.9721 | 0.9725 | 0.9576 | 0.9578 | 0.9123 | 0.9126 | 14.256 s |
| 0.03 | 0.9185 | 0.9189 | 0.9156 | 0.9160 | 0.9401 | 0.9409 | 15.126 s |
| 0.04 | 0.8472 | 0.8478 | 0.8312 | 0.8317 | 0.9721 | 0.9735 | 14.298 s |

**Table 5** The numerical comparison for skin friction with the existing literature, while keeping $\alpha = 1.0$, Pr = 6.2, $\beta = 1.0$, $\lambda =$, $Ec = 0.2$, $\phi_1 = \phi_2 = 0$.

| | Duwairi [34] | Tassaddiq et al. [2] | Present work |
|---|---|---|---|
| $f'(0)$ | 0.625 | 0.625100 | 0.625120 |
| $-g'(0)$ | 1.708 | −1.70803 | 1.70807 |
| $-\Theta'(0)$ | 2.264 | −2.26406 | −2.26411 |
| $-\Phi'(0)$ | | −0.78555 | −0.78559 |

ordinary system of differential equations is tackled through Fde12 and bvp4c. The main findings of this study are listed below:

- The rising trend of porosity term $\lambda$ reduces the flow field because the suction/injection takes place with the variation of $\lambda$, which resist to the flow field.
- The increment in Forchheimer term *Fr* decreases the fluid velocity. The porous surface permeability declines with the rising trend of Forchheimer term *Fr*. Which minimizes the velocity profiles of both Silver and Magnesium-oxide nanoliquid.
- The addition of nanoparticles in base fluid significantly enhances the viscosity of the fluid, while reduces the thermal expansion of the fluid, that's why the fluid velocity decreases with the variation of volume friction parameters ($\phi_1$, $\phi_2$).
- The thermal slip parameter reduces the friction force; those forces opposed to the flow field, and were the main agent for enhancing the temperature rate. That's why the temperature field declines with thermal slip parameter $\beta$ effects.
- The kinematic viscosity of fluid enhances with the effect of Schmidt number, which reduces the mass transmission rate.
- The fractional Matlab package fde12 and numerical technique bvp4c show best settlement at $\alpha = 1$.

## Declaration of Competing Interest

The authors declare that they have no known competing financial interests or personal relationships that could have appeared to influence the work reported in this paper.

## Acknowledgment

The authors extend their appreciation to the Deanship of Scientific Research at King Khalid University, Abha, Saudi Arabia for funding this work through research groups program under grant number R.G.P-2/97/42.

## References

[1] M. Shuaib, R.A. Shah, M. Bilal, Variable thickness flow over a rotating disk under the influence of variable magnetic field: an application to parametric continuation method, Adv. Mech. Eng. 12 (6) (2020), 1687814020936385.
[2] A. Tassaddiq, S. Khan, M. Bilal, T. Gul, S. Mukhtar, Z. Shah, E. Bonyah, Heat and mass transfer together with hybrid nanofluid flow over a rotating disk, AIP Adv. 10 (5) (2020) 055317.
[3] C. Zemedu, W. Ibrahim, Nonlinear convection flow of micropolar nanofluid due to a rotating disk with multiple slip flow, Math. Prob. Eng. (2020).
[4] A. Wakeel, L.B. McCash, Z. Shah, R. Nawaz, Cattaneo-Christov heat flux model for second grade nanofluid flow with hall effect through entropy generation over stretchable rotating disk, Coatings 10 (7) (2020) 610.
[5] A. Hafeez, M. Khan, J. Ahmed, Flow of Oldroyd-B fluid over a rotating disk with Cattaneo-Christov theory for heat and mass fluxes, Comput. Methods Prog. Biomed. 191 (2020) 105374.
[6] A. Hafeez, M. Khan, J. Ahmed, Flow of magnetized Oldroyd–B nanofluid over a rotating disk, Appl. Nanosci. (2020).
[7] S. Suresh, K.P. Venkitaraj, P. Selvakumar, M. Chandrasekar, Effect of Al2O3Cu/water hybrid nanofluid in heat transfer, Exp. Therm. Fluid Sci. 38 (2012) 54–60.
[8] M.I. Khan, M.U. Hafeez, T. Hayat, M.I. Khan, A. Alsaedi, Magneto rotating flow of hybrid nanofluid with entropy generation, Comput. Methods Programs Biomed. 183 (2020) 105093.
[9] N.S. Anuar, N. Bachok, I. Pop, Radiative hybrid nanofluid flow past a rotating permeable stretching/shrinking sheet, Int. J. Numer. Meth. Heat Fluid Flow (2020).
[10] J. Zhang, C. Cao, S. Zheng, W. Li, B. Li, X. Xie, Poly (butylene adipate-co-terephthalate)/magnesium oxide/silver ternary composite biofilms for food packaging application, Food Packag. Shelf Life 24 (2020) 100487.
[11] U. Gulati, U.C. Rajesh, D.S. Rawat, J.M. Zaleski, Development of magnesium oxide–silver hybrid nanocatalysts for synergistic carbon dioxide activation to afford esters and heterocycles at ambient pressure, Green Chem. 22 (10) (2020) 3170–3177.
[12] K. Saravanakumar, M.H. Wang, Biogenic silver embedded magnesium oxide nanoparticles induce the cytotoxicity in human prostate cancer cells, Adv. Powder Technol. 30 (4) (2019) 786–794.
[13] M. Goyal, H.M. Baskonus, A. Prakash, Regarding new positive, bounded and convergent numerical solution of nonlinear time

fractional HIV/AIDS transmission model, Chaos, Solitons Fractals 139 (2020) 110096.
[14] W. Gao, H. Günerhan, H.M. Baskonus, Analytical and approximate solutions of an epidemic system of HIV/AIDS transmission, Alexandria Eng. J. 59 (5) (2020) 3197–3211.
[15] A. Salem, F. Alzahrani, M. Alnegga, Coupled system of nonlinear fractional Langevin equations with multipoint and nonlocal integral boundary conditions, Math. Prob. Eng. (2020).
[16] D. Baleanu, A. Jajarmi, H. Mohammadi, S. Rezapour, A new study on the mathematical modelling of human liver with Caputo-Fabrizio fractional derivative, Chaos, Solitons Fractals 134 (2020) 109705.
[17] M. Shuaib, M. Bilal, M.A. Khan, S.J. Malebary, Fractional analysis of viscous fluid flow with heat and mass transfer over a flexible rotating disk, Comput. Model. Eng. Sci. 123 (1) (2020) 377–400.
[18] N.H. Tuan, H. Mohammadi, S. Rezapour, A mathematical model for COVID-19 transmission by using the Caputo fractional derivative, Chaos, Solitons Fractals 140 (2020) 110107.
[19] T. Akram, M. Abbas, M.B. Riaz, A.I. Ismail, N.M. Ali, An efficient numerical technique for solving time fractional Burgers equation, Alexandria Eng. J. (2020).
[20] N. Khalid, M. Abbas, M.K. Iqbal, D. Baleanu, A numerical investigation of Caputo time fractional Allen-Cahn equation using redefined cubic B-spline functions, Adv. Diff. Eqs. (2020) 1–22.
[21] R.M. Jena, S. Chakraverty, D. Baleanu, A novel analytical technique for the solution of time-fractional Ivancevic option pricing model, Phys. A Stat. Mech. Appl. 550 (2020) 124380.
[22] N. Khalid, M. Abbas, M.K. Iqbal, J. Singh, A.I.M. Ismail, A computational approach for solving time fractional differential equation via spline functions, Alexandria Eng. J. 59 (5) (2020) 3061–3078.
[23] T. Akram, M. Abbas, A. Iqbal, D. Baleanu, J.H. Asad, Novel numerical approach based on modified extended cubic B-spline functions for solving non-linear time-fractional telegraph equation, Symmetry 12 (7) (2020) 1154.
[24] I. Ameen, D. Baleanu, H.M. Ali, An efficient algorithm for solving the fractional optimal control of SIRV epidemic model with a combination of vaccination and treatment, Chaos, Solitons Fractals 137 (2020) 109892.
[25] W. Gao, P. Veeresha, D.G. Prakasha, H.M. Baskonus, G. Yel, New approach for the model describing the deathly disease in pregnant women using Mittag-Leffler function, Chaos, Solitons Fractals 134 (2020) 109696.
[26] Al.R. Mohammed, Maximum principles for nonlinear fractional differential equations in reliable space, Prog. Fract. Diff. Appl. 6 (2) (2020) 95–99.
[27] M.Z. Ullah, S. Serra-Capizzano, D. Baleanu, A numerical simulation for Darcy-Forchheimer flow of nanofluid by a rotating disk with partial slip effects, Front. Phys. 7 (2020).
[28] A. Aziz, A. Alsaedi, T. Muhammad, T. Hayat, Numerical study for heat generation/absorption in flow of nanofluid by a rotating disk, Results Phys. 8 (2018) 785–792.
[29] Y. Ma, R. Mohebbi, M.M. Rashidi, Z. Yang, MHD convective heat transfer of Ag-MgO/water hybrid nanofluid in a channel with active heaters and coolers, Int. J. Heat Mass Transf. 137 (2019) 714–726.
[30] K. Vajravelu, K.V. Prasad, J. Lee, C. Lee, I. Pop, R.A. Van Gorder, Convective heat transfer in the flow of viscous Ag–water and Cu–water nanofluids over a stretching surface, Int. J. Therm. Sci. 50 (5) (2011) 843–851.
[31] R. Davarnejad, M. Jamshidzadeh, CFD modeling of heat transfer performance of MgO-water nanofluid under turbulent flow, Eng. Sci. Technol. Int. J. 18 (4) (2015) 536–542.
[32] M.J. Uddin, O.A. Bég, N. Amin, Hydromagnetic transport phenomena from a stretching or shrinking non-linear nano material sheet with navier slip and convective heating: a model for bio-nano-materials processing, J. Magn. Magn. Mater. 368 (2014) 252–261.
[33] D. Ramya, R.S. Raju, J.A. Rao, A.J. Chamkha, Effects of velocity and thermal wall slip on magnetohydrodynamics (MHD) boundary layer viscous flow and heat transfer of a nanofluid over a non-linearly-stretching sheet: a numerical study, Propul. Power Res. 7 (2) (2018) 182–195.
[34] H.M. Duwairi, R.A. Damseh, Magnetohydrodynamic natural convection heat transfer from radiate vertical porous surfaces, Heat Mass Transfer 40 (10) (2004) 787–792.